Efficient CeO_2 and CeO_2-Al_2O_3 supports for Ru as 3rd generation ammonia synthesis catalysts: enhanced kinetic mechanism over commercial Ru/CeO_2

ABSTRACT

In order to make the ammonia synthesis process more sustainable and facilitate its coupling with renewable energies, it is first imperative to carry out this reaction at lower temperatures, which requires new catalysts showing high activity (i.e., low activation energies) and proper kinetic characteristics (e.g., resistance to H_2 and NH_x poisoning) while operating at these temperature conditions. While Ru presents high activity in this reaction, it suffers from strong hydrogen inhibition, which is particularly important at low temperatures. The use of promoters such as cerium oxide can mitigate this issue taking advantage of metal-support interactions generated upon reduction treatments (e.g., electron donation and the formation of new oxygen vacancy sites). However, lab-synthesized ceria materials usually present low surface areas, thereby limiting the generation of oxygen vacancies and the ammonia synthesis activity as a result of weak metal-support interactions. With the aim of overcoming this issue, we prepared, by a simple impregnation method, high surface area ceria- and ceria-alumina-supported Ru catalysts with improved ammonia synthesis performance at moderate temperatures. In this sense, lab-synthesized Ru/CeO_2 (with higher specific surface area and lower crystallinity than commercial ceria) showed stronger metal-support interactions than the commercial sample, which resulted in a superior global ammonia synthesis kinetic mechanism with more positive hydrogen reaction orders (i.e., more resistant to hydrogen inhibition) and significantly lower activation energies (46 vs 61 kJ mol^{-1}). We

found that the use of alumina as structural support increased the surface area of ceria, thereby promoting the Ru-CeO_2 interaction and the catalytic performance. We analyzed the effect of the surface chemistry of two different commercial aluminas (acid and basic) with similar surface areas. Basic alumina was found to increase the specific surface area of the catalyst to a larger extent as compared to acid alumina. Thus, the Ru/CeO_2-Al_2O_3 catalyst with a 50 wt% of basic alumina showed an ammonia synthesis activity of 1.9 mmol g h^{-1} at 400 °C and ambient pressure and an activation energy as low as 44.8 kJ mol^{-1}.

Keywords: Ammonia synthesis; Low activation energy; Metal-support interactions; High surface ceria; ceria-alumina; basicity

1. Introduction

The change in the global energy paradigm during the last decades shows a scenario in which green ammonia (NH_3) could be used as a chemical platform for decentralized green hydrogen (H_2) plants [1–3]. The current industrial process producing NH_3 from H_2 is incompatible with the use of renewables since harsh temperature (400-600 °C) and pressure (20-60 MPa) conditions are required to produce ammonia [4]. Such high temperatures are required to activate the N_2 molecule and break the stable N≡N triple bond. Thus, high pressures are on demand in order to circumvent both kinetic and thermodynamic limitations since the ammonia synthesis reaction is highly exothermic (ca. -92 kJ $mol^{-1}_{NH_3}$) [5].

Therefore, to successfully complete the transition into the new global green hydrogen scenario, the ammonia synthesis process needs to overcome several challenges, mainly related to the catalytic reaction system [6,7]. In this context, several alternatives to the conventional thermocatalytic ammonia synthesis process are being proposed by the research community, including plasma [8,9], mechanocatalytic synthesis [10], chemical looping [11–13], photothermal catalysis [14] and electrocatalytic synthesis [15,16].

However, given the early stage of research of these processes, the investigation efforts to design efficient catalysts for thermocatalytic ammonia synthesis at mild conditions have also grown exponentially within the last two decades [17–19]. The most recent works are focused on the development of stable and efficient catalysts based on non-noble metals, although the complex synthesis methods and conditions required represent a handicap for their application scalability [20,21]. In this sense, most novel catalysts mainly rely on the performance of complex and sometimes non-stable functional supports such as electrides, hydrides, nitrides or intermetallics [17–

19,22–25], which limits its practical applicability.

Rare earth metal oxides have been reported to present excellent electronic properties under strong metal support interaction (SMSI) conditions, i.e., they can serve as electron donors for the transition metal (TM), thereby promoting nitrogen dissociation, which is usually the rate determining step (RDS) of the process [26]. Cerium oxide, the most abundant rare earth oxide, forms oxygen vacancies upon reduction, thereby promoting the metal (e.g., Ru, Co) by forming new interfacial metal-CeO_{2-x} sites [27] for the ammonia synthesis and promoting metal electronic donation. Thus, Ru/CeO_2 based catalysts have been reported to be more efficient than 1st generation Fe-based and 2nd generation Ru-based catalysts such as Ru/MgO or Ru/C [19].

However, commercial ceria usually suffers from low surface area, which reduces the extent of the metal-support interaction and ultimately results in apparent activation energies significantly higher as compared to catalysts based on novel supports such as electrides and hydrides [17,18]. Therefore, the design of ceria-based catalysts with higher surface area and optimum metal-support interaction can increase both the number and activity of Ru sites in the ammonia synthesis reaction. One of the methods to increase the surface of ceria is the use of a high surface area material as a structural support. In this sense, alumina (Al_2O_3) is a widely used structural support in many applications in the field of thermocatalysis, since it has optimal structural properties. With regards to the ammonia synthesis, Al_2O_3 has been used as a structural promoter for Fe and some attempts were also made for Ru. However, it was concluded that acid sites from alumina can strongly interact with the NH_3 molecule, hindering its desorption [22]. Therefore, basic supports, such as rare earth-based materials are usually preferred as structural promoters [28]. Also, considering that the SMSI between Ru and CeO_2

mainly takes place on the catalyst surface [29], it could be interesting to substitute a fraction of the ceria-based support by cheaper alumina, as long as the support surface could be covered by ceria.

In this work, we analyse the differences in terms of performance between two different materials as supports for Ru: a commercial ceria (to be named as $CeO_2|_C$) and a cerium oxide made by a simple impregnation-calcination method from cerium nitrate (to be named lab-synthesized cerium oxide: $CeO_2|_{AS}$). We demonstrate that lab-synthesized ceria outperforms commercial ceria as a result of its higher surface area and lower crystallinity, which led to the formation of a higher concentration of more reactive surface oxygen vacancies. The impregnation-calcination synthesis method used herein allowed to prepare a ceria support with improved kinetic properties in the ammonia synthesis reaction as compared to commercial ceria.

Furthermore, we study the impact of the structural promotion of ceria with two types of different Al_2O_3 materials using a similar impregnation-calcination procedure. We found that the acid sites of γ-Al_2O_3 played a detrimental role in the performance of the Ru/CeO_2-Al_2O_3 catalysts, whereas basic Al_2O_3 allowed to improve the kinetic performance of Ru/CeO_2.

2. Experimental

2.1. Catalyst preparation

Lab-synthesized ceria support was prepared using an aqueous solution of $Ce(NO_3)_3 \cdot 6H_2O$ (99 wt % trace metal basis, Sigma-Aldrich). After the complete dissolution of cerium nitrate, the solution was evaporated overnight and the resulting solid was calcined at 400 °C for 6 h (2 K min^{-1}). Cerium oxide was softened by hand-milling with an agate mortar.

Ceria-alumina supports were prepared by aqueous impregnation of

$Ce(NO_3)_3 \cdot 6H_2O$ in an aqueous suspension of any of two different aluminium oxide materials: basic alumina (activated basic, Brockmann I, Sigma-Aldrich) and acid alumina (anhydrous γ-alumina, Merck). The impregnation was carried out by stirring the suspension at room temperature for 6 h. After the impregnation and subsequent overnight evaporation, the support materials were calcined at 400 °C for 6 h (2 K min^{-1}) and then softened by hand-milling with an agate mortar.

Ruthenium (III) acetylacetonate (Ruacac 97 %, Sigma-Aldrich) was used as Ru precursor. The catalysts with a 5 wt % loading of Ru were prepared by impregnation of Ruacac onto the supports previously synthesized in ethanol. After impregnation, the suspensions were evaporated, and the catalysts were homogenized using an agate mortar. A pre-reduction treatment was applied to all the catalysts, following previously reported methods [30].

2.2. Kinetic experiments

The kinetic tests were carried out in a micro-reaction system with automated integral pressure, temperature, gas flow and composition control (Microactivity-Effi, PID, Micromeritics) in a 316SS fixed-bed reactor. A stoichiometric N_2/H_2 (1:3) flow of 60 NmL min^{-1} with a catalyst loading of 0.1 g and a space velocity of 36000 mL g^{-1} h^{-1}. To ensure that the reaction conditions are far away from equilibrium limitations, the base case is set up at 400 °C and atmospheric pressure. For the calculation of N_2 and H_2 reaction orders, He was used as an inert diluent gas. With the aim of obtaining accurate temperature measurements, a thermocouple was placed into the catalyst bed. The produced ammonia was trapped in an aqueous solution of diluted sulfuric acid (5 mM) and ammonium ion (NH_4^+) was measured by means of an ion chromatograph (Dionex Easion, Thermo Scientific).

The reproducibility of the kinetic experiments was checked as follows: a repetition

of the whole kinetic mapping for each catalyst was carried out in different runs until the values of the ammonia reaction rate at the base case conditions and the activation energies showed a standard deviation below a 10 % over the average.

The procedure for the calculation of the reaction orders is shown in the supporting information, section S1.

2.3. Characterization

Nitrogen physisorption experiments measurements (ASAP 2020 Plus, Micromeritics) were used to obtain the Brunauer–Emmet–Teller (BET) specific surface areas of the catalysts. Crystalline patterns were analysed by means of an X-ray diffraction (XRD, Bruker D8-Advance) with Cu Kα radiation. X-ray Fluorescence (XRF, Zetium de PANalytical) was carried out to measure the bulk composition of all the catalysts. Surface analyses were done by means of X-ray Photoelectron Spectroscopy (XPS, NEXSA, Thermo-Scientific), using a monochromatized Mg-Kα radiation. Binding energies were calibrated with the carbon C-C 1s bind (284.6 eV). H_2 Temperature Programmed Reduction (H_2-TPR) analyses were done to study the SMSI and the formation of oxygen vacancies. A gas flow of 100 mL min^{-1} with a composition of 5 % H_2 into He was used, with a heating ramp of 10 °C min^{-1}. The outlet gas composition was measured by a mass spectrometer (Omnistar GSD 301 O_2, Pfeiffer Vacuum). High-Angle Annular Dark-Field Scanning Transmission Electron Microscopy (HAADF-STEM) experiments were conducted in a Talos F200X (Thermo Fisher Scientific) microscope, with a High-Resolution scanning (HRSTEM: 0.16 nm @200 kV).

3. Results and discussion

3.1. Lab-synthesized ceria vs commercial ceria

The N_2 physisorption results for both commercial and lab-synthesized ceria-based

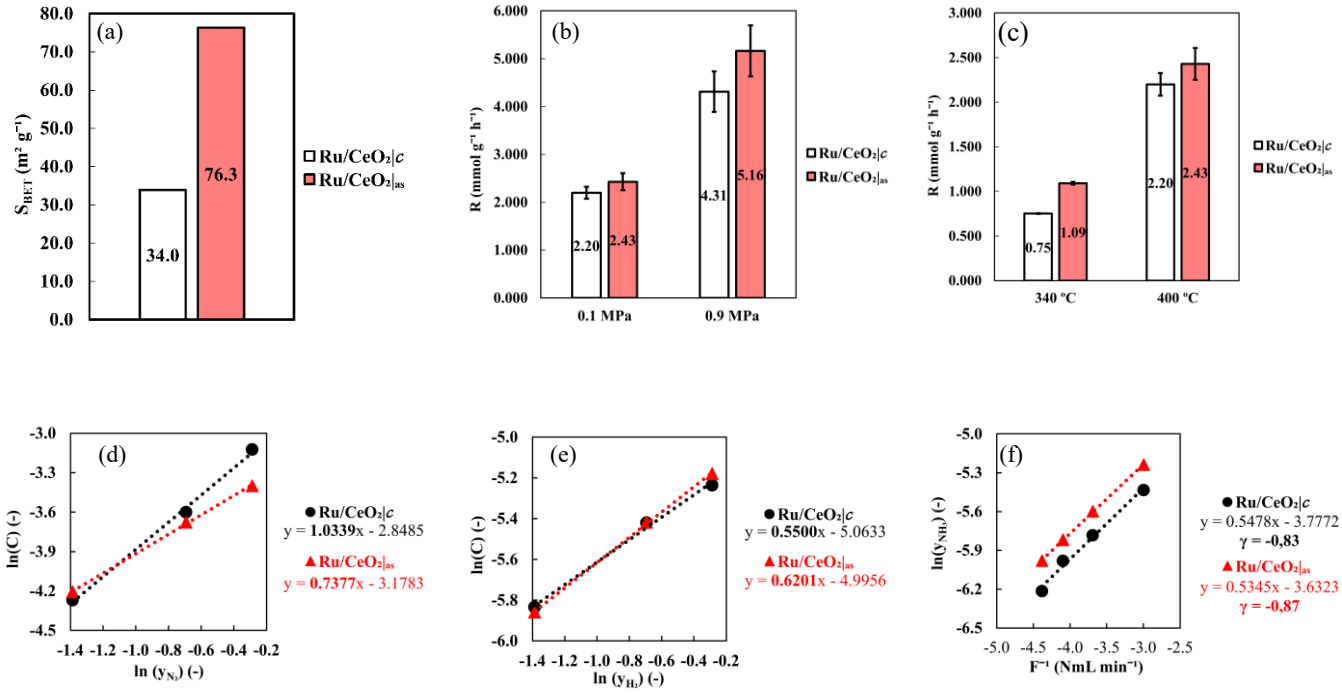

Fig. 1. (a) Specific surface area of $Ru/CeO_2|_C$ and $Ru/CeO_2|_{AS}$; (b) Ammonia synthesis rates at 0.1-0.9 MPa and 400 °C; (c) Ammonia synthesis rates at 340-400 °C and 0.1 MPa; (d) Nitrogen reaction order (α) plot, determined at 400 °C and 0.1 MPa; (e) Hydrogen reaction order (β) plot, determined at 400 °C and 0.1 MPa; (f) Ammonia reaction order (γ) plot, determined at 400 °C and 0.1 MPa.

catalysts are shown in Fig. 1a. The simple impregnation-calcination synthesis method used herein resulted in a material with significantly higher specific surface area as compared to the commercial sample (76.3 vs 34.0 m^2 g^{-1}). This difference in the specific surface area is important since the catalytic activity of Ru-based catalysts in this reaction has been found to be strongly influenced by the metal shape and particle size [31,32], as well as by the support morphology [29]. Interestingly, the specific surface area obtained for $Ru/CeO_2|_{AS}$ was higher than other typical ceria-based catalysts (Table S1), which highlights the success of our simple impregnation-calcination synthesis.

Ammonia synthesis rates for both catalysts at low and high pressure are shown in Fig. 1b. $Ru/CeO_2|_{AS}$ showed slightly higher activity than $Ru/CeO_2|_C$ at 0.1 MPa (2.43 vs 2.20 mmol g^{-1} h^{-1}). Both values were higher than those reported for other Ru/CeO_2 catalysts under the same operating conditions [27]. The performance gap between both

catalysts further increased to 20 % at higher pressures (5.16 mmol g^{-1} h^{-1} for $Ru/CeO_2|_{AS}$ and 4.31 mmol g^{-1} h^{-1} for $Ru/CeO_2|_C$). This pressure effect is intimately related to the kinetic efficiency, in particular, to the resistance towards hydrogen poisoning [33]. Thus, these results revealed a more efficient global kinetic mechanism for $Ru/CeO_2|_{AS}$ [21,34].

The effect of the operating temperature over the ammonia synthesis performance was studied by performing runs at 400 (base case) and 340 °C (Fig. 1c). The relative difference in terms of performance between both catalysts was 4-fold higher at 340 °C, as compared to that observed at 400 °C. The Arrhenius analysis revealed an activation energy of 61.3 kJ mol^{-1} for $Ru/CeO_2|_C$ (Fig. S3b), while a noticeably low value of 46.1 kJ mol^{-1} was obtained for $Ru/CeO_2|_{AS}$ (Fig. S3f). This activation energy was significantly lower than those reported for other similar Ru/CeO_2 catalysts (Table S1) and comparable to those of the best ammonia synthesis 3rd generation catalysts such as complex single atom catalysts (SACs), intermetallics and hydrides [17–19,27]. This outstanding performance highlights the success of the simple synthesis method used herein.

In the case of those catalysts following a dissociative mechanism, such as Ru/CeO_2, it is well known that the lower the activation energy, the more efficient is the N_2 dissociation and activation step, which is usually the RDS of the reaction [18,35–37]. This was further confirmed by the N_2 reaction order analysis. Typical N_2 (α), H_2 (β) and NH_3 (γ) reaction orders plots are shown in Fig. 1d, Fig. 1e and Fig. 1f, respectively. While β and γ were similar for both catalysts, α was 29% lower for $Ru/CeO_2|_{AS}$ [35] compared to $Ru/CeO_2|_C$, revealing a lower importance of the N_2 dissociation step for $Ru/CeO_2|_{AS}$. It is also remarkable that β was positive for both catalysts which suggests that hydrogen poisoning is not relevant over these catalysts, in line with the positive pressure effect shown in Fig. 1b [38]. Interestingly, $Ru/CeO_2|_{AS}$ showed higher β values

than the commercial sample (0.62 vs 0.55, Fig. 1e), thereby revealing a higher resistance to hydrogen inhibition over this catalysts. Moreover, the highly negative values of γ (ca. -0.8) indicate that NH_3 is prone to be absorbed over the catalysts so that the formation of NH_x species (rather than the N_2 dissociation step) play a crucial role in the global kinetic scheme [38].

With the aim to gain insight into the reasons for the different performance of $Ru/CeO_2|_{AS}$ and $Ru/CeO_2|_C$, further characterization was carried out. Since the specific surface area of $Ru/CeO_2|_{AS}$ was significantly higher than that of the commercial sample, it is expected ceria to have lower particle size in this sample, leading to an improved metal-support interaction upon reduction [39].

An analysis of the Ru dispersion was carried out by means of HAADF-STEM with EDX mapping (Fig. 2a and Fig. 2b). Ru was found to be well dispersed over CeO_2 for both catalysts, although the lab-prepared sample showed optimum dispersion results (Fig. 2b). HAADF-STEM pictures for all the catalysts characterized in this work are shown in Fig. S1, whereas the EDX mapping with the contrast between Ru and Ce is shown in Fig. S2. $Ru/CeO_2|_C$ (Fig. S1a) was found to present an organized structure in the form of nanoplatelets, whereas $Ru/CeO_2|_{AS}$ (Fig. S1e) seems more amorphous. The $Ru/CeO_2|_{AS}$ sample showed minor Ru agglomeration, which can be ascribed to the simplicity of the synthesis method.

These results were further confirmed by XRD (Fig. 2c). The crystalline pattern showed peaks corresponding to the fluorite structure of CeO_2, which means that the support preserves the original Ce^{4+} crystalline lattice after the pre-reduction process. $Ru/CeO_2|_{AS}$ showed less intense and wider diffraction peaks than $Ru/CeO_2|_C$, revealing a lower crystallinity. In order to quantify the difference in the crystallinity between both catalysts, the crystallite sizes of the first peak i.e., $2\Theta = 28.5°$ were obtained using the

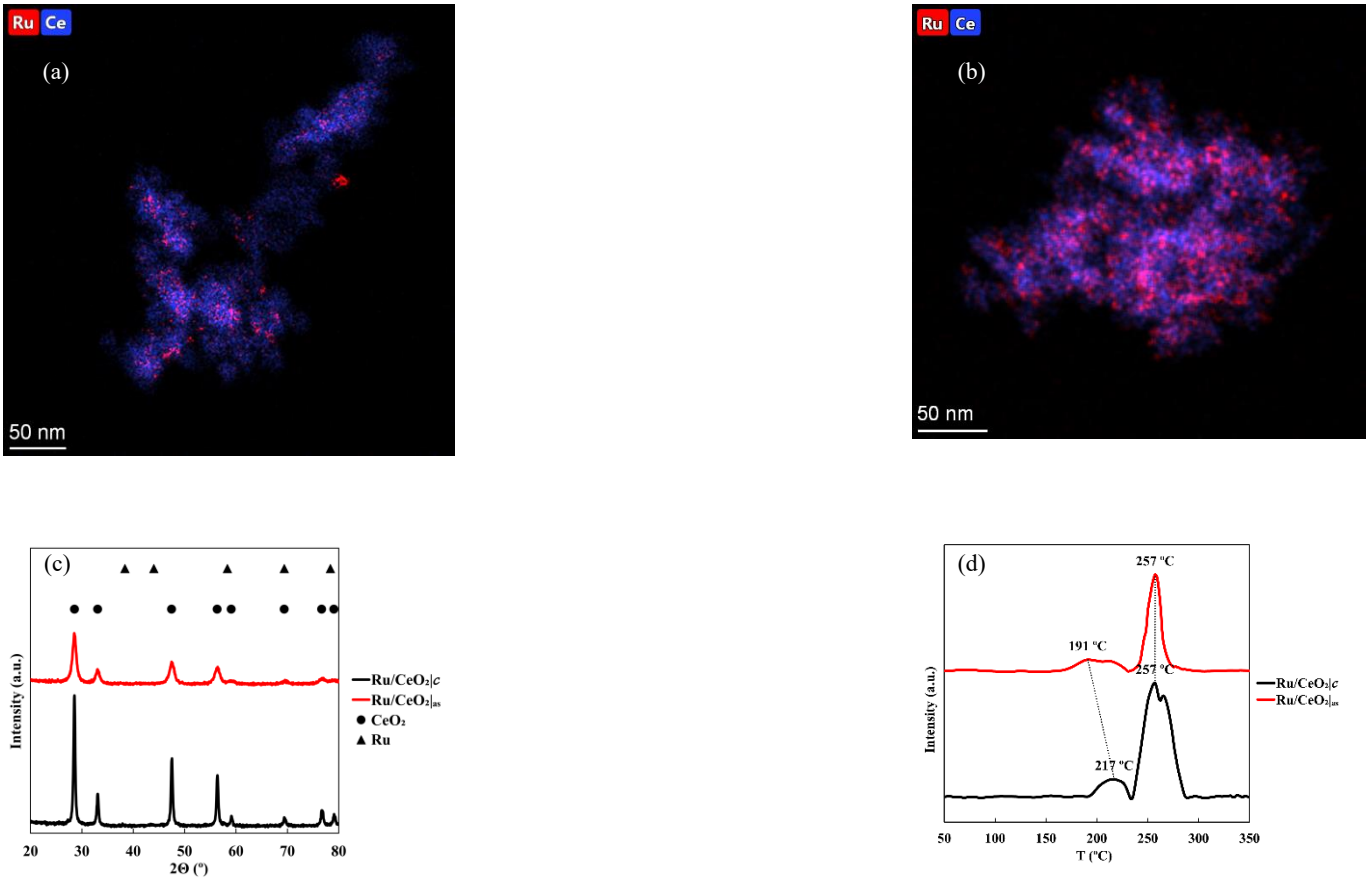

Fig. 2. Ru coupled to Ce elemental EDX mapping from HAADF-STEM results of (a) commercial ceria catalyst and (b) as-synthesized ceria catalyst; (c) XRD patterns; (d) H_2-TPR profiles.

Scherrer equation shown in Eq. (1).

$$D_C = \frac{K \cdot \lambda}{\beta \cdot \cos\Theta} \quad (1)$$

where "D_C" is the crystallite size, "K" is the shape factor (a value of 0.9 was taken as an approximation in this case), "λ" is the X-ray wavelength, "β" is the full width at half maximum (FWHM) of the peak and "Θ" is the peak angle (half of 2Θ). Since the key point is a comparison between the crystallite size for both catalysts, an arbitrary value of 0 was taken for the instrumental line broadening, which leads to an approximation of the values of the crystallite sizes. As expected, $RuCeO_2|_C$ showed significantly higher CeO_2 crystallite size than the $RuCeO_2|_{AS}$ sample (22.8 vs 9.4 nm). As reported in previous studies, the lower the crystallinity, the higher the presence of structural defects. These results are in line with the improved kinetic mechanism for

ammonia synthesis of the lab-synthetized sample as a result of an optimum Ru-CeO_2 contact [40].

In order gain insight into the Ru-CeO_2 interaction, H_2-TPR experiments were conducted, from which the generation of oxygen vacancies and the specific role of the interactions between Ru and CeO_2 can be inferred. H_2 (m/z = 2) profiles for both catalysts are shown in Fig. 2d. No reduction peaks were found at temperatures typical of the reduction of Ru oxides [41] (below 180 °C), revealing that Ru is in the form of Ru^0. The fact that Ru is not present as oxidized species can explain the absence of large Ru particles and agglomerations revealed by TEM (Fig. 2a and Fig. 2b). Thus, the preparation method used herein led to well dispersed Ru particles avoiding the formation of Ru oxides patches which are typical of impregnation-calcination processes [22]. Two main reduction peaks were observed in the TPR profiles: one at low temperature (< 250 °C) peak was attributed to the reduction of surface ceria in intimate contact with Ru, whereas the peak at higher temperature (>250 °C) corresponded to the reduction of surface ceria not in close contact with Ru. The reduction of surface ceria in close contact with Ru can be associated with SMSI between Ru and CeO_2 [29]. By comparing the TPR profiles of the catalysts and the supports (Fig. S3a), it can be inferred that Ru improved the reducibility of ceria, most likely by a hydrogen spillover process [42]. Ru/$CeO_2|_{AS}$ showed lower reduction temperatures for surface CeO_2 in contact with Ru as compared to Ru/$CeO_2|_C$ (191 vs 217 ºC, Fig. 2d). These results revealed a more intense metal-support interaction for Ru/$CeO_2|_{AS}$ and, potentially, an enhanced electron transfer between CeO_2 and Ru, which could account for its superior activity and the different kinetic mechanism of both catalysts [40]. Reduction of the surface CeO_2 not closely in contact with Ru took place at a similar temperature for both catalysts (257 °C).

In conclusion, the simple impregnation-calcination method used herein led to the formation of a low crystallinity cerium oxide with a higher surface area, as compared to the commercial ceria. $Ru/CeO_2|_{AS}$ showed a high degree of crystalline defects, which promotes the formation of more active surface oxygen vacancies for those CeO_2 active sites in contact with Ru, showing an enhanced SMSI. This enhanced catalyst showed an outstanding performance for low-temperature ammonia synthesis (e.g., low activation energy) and a more efficient kinetic mechanism.

3.2. Structural promotion with basic and acid alumina

As explained in the previous section, the formation of a high surface low-crystallinity cerium oxide resulted in a Ru/CeO_2 catalysts with improved metal-support interaction and excellent low-temperature ammonia synthesis performance. With the aim to increase the surface area of the cerium oxide and enhance the $Ru\text{-}CeO_2$ interaction, we used alumina as a structural support. Two different aluminium oxide materials with similar specific surface areas (basic and acid) were used as structural promoters.

The nomenclature of the samples is shown in Table 1, with samples S1 and S5 being respectively $Ru/CeO_2|_{C}$ and $Ru/CeO_2|_{AS}$ described in the previous section. The specific surface area of the samples is shown in Fig. 3a as a function of the ceria loading. As shown in Fig 3a, the utilization of small amounts of alumina (e.g., 20 wt%) resulted in a significant increase in the BET surface area, especially for basic alumina. In the case of acid alumina, the specific surface area of the catalyst remained nearly unchanged as the alumina loading increased from 20 to 80 wt%.

Table 1. Nomenclature of $Ru/CeO_2\text{-}Al_2O_3$ catalysts

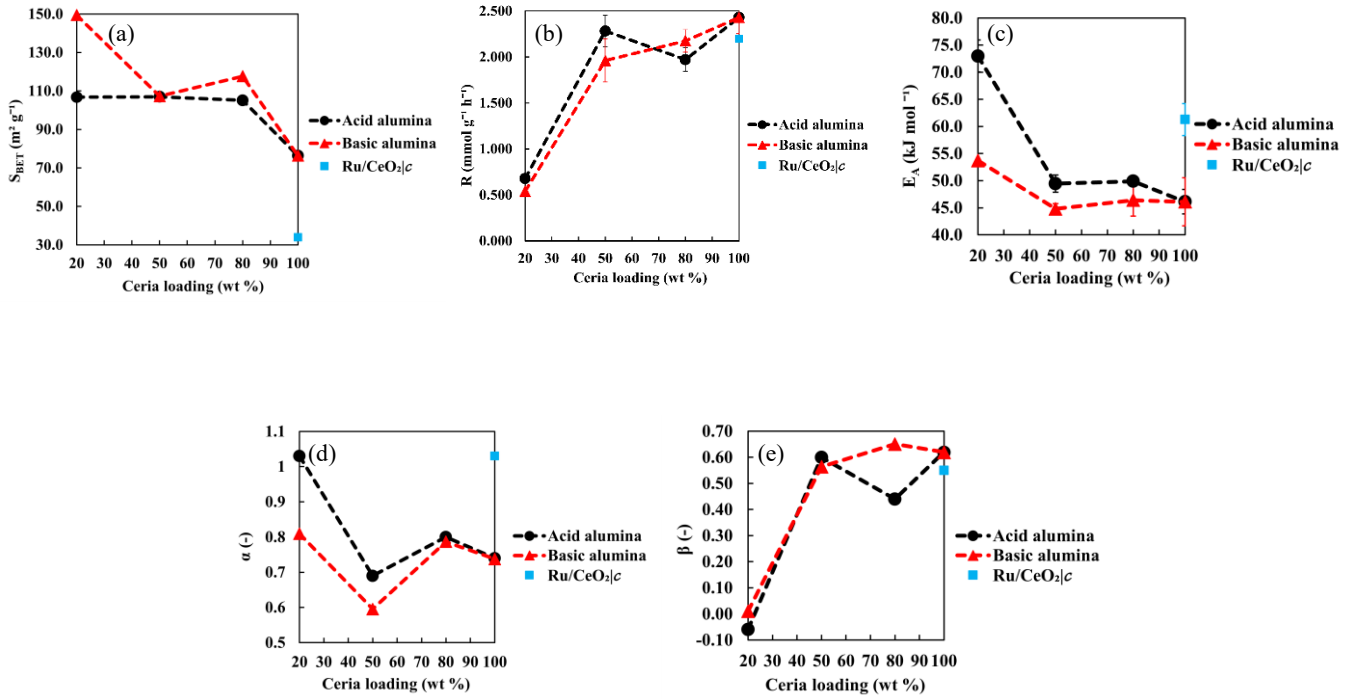

Fig. 3. (a) Specific surface area of Ru/CeO_2-Al_2O_3 catalysts as a function of the ceria loading; (b) Ammonia synthesis rates in the base case conditions as a function of the ceria loading; (c) Activation energies at 400 °C and 0.1 MPa as a function of the ceria loading; (d) Nitrogen reaction order at 400 °C and 0.1 MPa as a function of the ceria loading; (e) Hydrogen reaction order at 400 °C and 0.1 MPa as a function of the ceria loading.

Sample	Alumina	Ceria	CeO_2 (wt %)
S1	-	Commercial	100
S2	Acid	Lab-synthesized	20
S3			50
S4			80
S5	-		100
S6	Basic		20
S7			50
S8			80

The activity of the Ru/CeO_2-Al_2O_3 catalysts in the ammonia synthesis reaction was measured as a function of the ceria loading (Fig. 3b) under base case conditions (400 °C and 0.1 MPa). In the case of basic alumina, the ammonia synthesis rate increased continuously with the ceria loading, with a maximum value of 2.18 mmol g^{-1} h^{-1} for the

sample with 80 wt% of ceria. In the case of the acid alumina, the sample with 50 wt% of ceria showed an optimum activity (2.28 mmol g^{-1} h^{-1}) and only slightly lower than that of the pure ceria sample $Ru/CeO_2|_{AS}$ (S5) despite containing half of the ceria loading. These results also revealed that ceria plays a key role in promoting the ammonia synthesis reaction on Ru. In fact, once the ceria loading is reduced to 20 wt%, the ammonia synthesis rate decreased considerably, reaching values in the 0.5-0.7 mmol g^{-1} h^{-1} range for both basic and acid alumina catalysts. This decrease can be explained by Ru-Ce sites being partially replaced with Ru-Al sites, which are not active considering that alumina is not a functional support for Ru [43].

Significant differences were found in the kinetic behaviour of the catalysts for both aluminas. Thus, the catalysts supported on acid alumina showed higher activation energies than those supported on basic alumina and higher than that of $Ru/CeO_2|_{AS}$ (Fig. 3c). The Arrhenius plots for all the catalysts are shown in the Supporting Information (Fig. S3b–i). Interestingly, the activation energy of the 20 wt% ceria catalyst supported on acid alumina was as high as 73.0 kJ mol^{-1} (versus 53.7 kJ mol^{-1} for the same catalysts supported on basic alumina). This result seems to indicate that the acid sites of γ-alumina have a detrimental effect on the Ru-CeO_2 interaction, thereby increasing the apparent activation energy for the reaction. Also, as previously reported, acid sites on the support strongly adsorb the ammonia produced (i.e., ammonia poisoning), negatively affecting the global catalyst performance [28,44]. Basic alumina catalysts slightly outperformed $Ru/CeO_2|_{AS}$ in terms of an enhanced kinetic mechanism, with an optimum activation energy of 44.8 kJ mol^{-1} for a ceria loading of 50 wt %. This result is interesting in that 50% of ceria can be replaced with cheaper alumina with minimum effect on the activity and improved kinetic mechanism.

Nitrogen (α), hydrogen (β), and ammonia (γ) reaction orders are shown in Fig. S4a,

S4b and S4c, respectively. The dependence of α and β with the ceria loading is shown in Fig. 3d and Fig. 3e, respectively. For both acid and basic alumina, nitrogen reaction orders reached minimum values at a ceria loading of 50 wt % (0.69 and 0.60, respectively). Overall, catalysts supported on basic alumina showed lower nitrogen reaction orders than catalysts supported on acid alumina. These results are in line with the Arrhenius results (Fig. 3c) revealing a facilitated nitrogen dissociation and activation pathway for catalysts supported on basic alumina. Noticeably, the 50 wt% ceria catalyst supported on basic alumina showed lower nitrogen reaction orders than $Ru/CeO_2|_{AS}$ (0.60 vs 0.74). With regards to hydrogen reaction orders, positive values were obtained for ceria loadings higher than 50 wt%, thereby ruling out hydrogen inhibition (unlike catalysts with a 20 wt% of ceria).

HAADF-STEM pictures of the alumina-supported catalysts are shown in Fig. S1. Unlike $Ru/CeO_2|_C$, none of the Ru/CeO_2-Al_2O_3 catalysts seem to present a clearly defined structure, probably because of the poor crystallinity of both aluminas after the calcination process (Fig. S4d). Elemental EDX patterns of Ru and Ce (Fig. S2) revealed poorer Ru dispersion for the alumina-based catalysts as compared to $Ru/CeO_2|_{AS}$ (Fig. S2e).

XRD patterns of the CeO_2-Al_2O_3 samples (Fig. 4a) showed no evidences of Al_2O_3 phases, in line with the poor crystallinity of these materials. CeO_2 crystallite sizes (calculated by the Scherrer equation, Fig. 4b) similar to those of $Ru/CeO_2|_{AS}$ were found for ceria loadings of 50 and 80 wt%, with samples supported on basic alumina showing slightly lower ceria crystallite sizes than their acid alumina-supported counterparts. However, this difference seems to be marginal to explain the differences in terms of performance of both aluminas. Overall, the CeO_2 crystallite size for all the ceria-alumina based catalysts does not account for the different kinetic behaviour explained

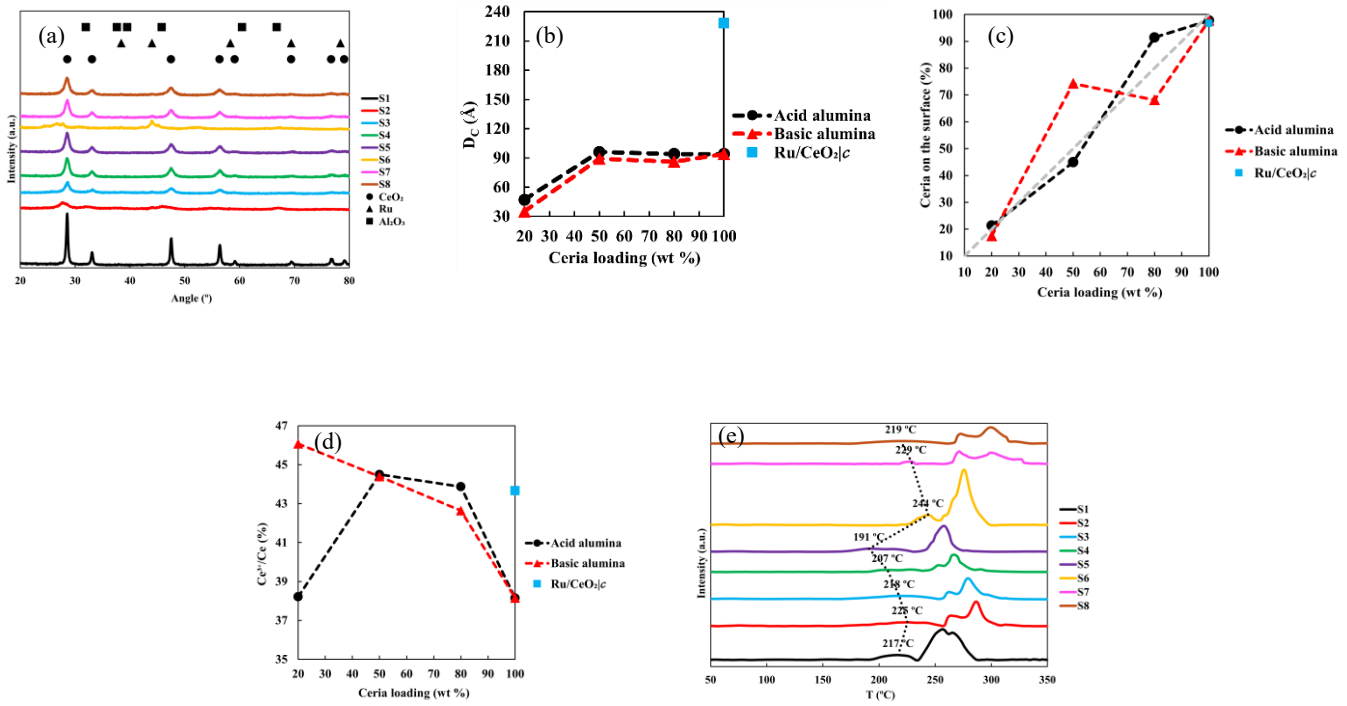

Fig. 4. Characterization of Ru/CeO_2-Al_2O_3 catalysts: (a) XRD patterns; (b) CeO_2 crystallite sizes; (c) Surface ceria content as a function of ceria loading determined by XPS; (d) Surface Ce^{3+} concentration as a function of ceria loading determined by XPS; (e) H_2-TPR profiles.

above.

As aforementioned, the SMSI is related to the Ru-Ce interactions at the catalyst surface. In order to study the distribution of the different elements on the catalyst surface and their oxidation state, X-ray photoelectron spectroscopy (XPS) analyses were conducted. The distribution of Al, Ce and Ru was calculated assuming that these elements were present on the surface in the form of Al_2O_3, CeO_2 and Ru^0, respectively, as an approximation, since those are the expected chemical species for Al, Ce and Ru, respectively. The amount of CeO_2 on the surface as a function of the ceria loading is shown in Fig. 4c. For acid alumina catalysts, there is a direct relation between the ceria loading and the amount of ceria present on the catalyst surface, with maximum deviations of 12 wt% between both parameters, thus revealing that cerium oxide is well dispersed over the alumina matrix. Conversely, the basic alumina catalysts with 50 wt%

loading showed the highest deviation between the ceria content on the catalyst surface and in the bulk, which could explain the good kinetic properties of this catalyst (e.g., low activation energy, low nitrogen reaction order and positive hydrogen reaction order). In order to gain insight into the reducibility of the ceria on these catalysts, a previously reported method was used to calculate the distribution of Ce^{3+} and Ce^{4+} from the deconvolved XPS patterns [45]. These results are shown in Fig. 4d, whereas the Ce 3d XPS patterns are shown in Fig. S5a. For basic alumina catalysts, the lower the ceria loading, the higher the amount of surface Ce^{3+}. In the case of acid alumina catalysts, the amount of surface Ce^{3+} reached a maximum for a ceria loading of 50 wt%, in line with the kinetic results revealing an optimum performance for this catalyst among the acid alumina-based materials. The low amount of surface Ce^{3+} obtained for the 20 wt% acid alumina catalyst is in line with the hypothesis that acid sites on alumina have a detrimental effect on the Ru-CeO_2 interaction.

XPS patterns for Ru are shown in Fig. S5b. For all the samples, the Ru $3p_{1/2}$ peak was attributed to Ru^{3+}species [46], while the $3p_{2/3}$ peak was assigned to Ru^0 [47]. XPS results revealed the presence of oxidized Ru species, probably upon air exposure after the pre-reduction treatment prior to XPS analyses. Slight deviations of the Ru $3p_{1/2}$ peaks over the values reported in literature were observed [46], which seems to indicate that Ru^0 is only partially oxidized by air exposure.

XRF (Fig. S5c) revealed similar tendencies than those observed for XPS results for surface ceria content. Furthermore, an effective Ru loading of 2-3 % was achieved for all the catalysts reported in this work, with no significant relation between Ru and CeO_2 loading (Fig. S5d) for both acid and basic alumina-based catalysts.

H_2-TPR profiles of the ceria-alumina catalysts (Fig. 4e) showed two main peaks at low and high temperatures which can be ascribed to the reduction of surface ceria in

close contact with Ru and surface ceria not in contact with Ru, respectively. The low temperature peaks appeared at lower temperatures as the ceria loading increased for both aluminas, with optimum values (207 and 219 ºC) for an 80 wt% ceria loading on acid and basic alumina, respectively. Interestingly, alumina-supported catalysts showed reduction peaks at higher temperatures compared to $Ru/CeO_2|_{AS}$ (S5, Fig. 4e) which seems to indicate that the presence of alumina affects the net formation of surface oxygen vacancies as a consequence of a less intense interaction between Ru and CeO_2, particularly for basic alumina. Therefore, it seems clear that the strength of the metal-support interaction for the CeO_2-Al_2O_3 catalysts depends highly on the ceria loading rather than on the surface area. For instance, the sample S8 showed reduction peaks at higher temperatures than the $Ru/CeO_2|_{AS}$ despite having significantly higher specific surface area.

As a summary, the role of alumina as a structural promoter for ceria in Ru/CeO_2-Al_2O_3 catalysts has been unveiled. The use of alumina as support allowed to generate a high surface area, low crystalline and highly dispersed reducible cerium oxide, which helped improve the ammonia synthesis mechanism by decreasing the apparent activation energy and the nitrogen reaction order, with optimum loadings of 50 wt% for both acid and basic alumina supports. Acid alumina had a negative effect on the catalytic performance, probably due to the strong adsorption of the ammonia produced in acid sites (ammonia inhibition). This poisoning effect was most relevant for low ceria loadings (e.g., 20 wt%). The Ru/CeO_2-Al_2O_3 catalyst with a 50 wt% ceria and basic alumina showed optimum kinetic performance with an activation energy as low as 44.8 kJ mol^{-1}.

4. Conclusions

A simple impregnation-calcination method was used herein for the synthesis of

CeO_2 and CeO_2-Al_2O_3 supports for Ru. These catalysts showed an outstanding performance for the low-temperature ammonia synthesis reaction, with activation energies comparable to those of the best catalysts reported so far. In this sense, a lab-prepared high-surface-area sample Ru/$CeO_2|_{AS}$ showed an activation energy as low as 46.1 kJ mol^{-1}. This sample also showed excellent low-temperature kinetic behaviour with very positive H_2 reaction orders (thereby avoiding typical hydrogen inhibition issues associated with Ru) and significantly lower N_2 reaction order as compared to a commercial counterpart (thereby allowing enhanced N_2 dissociation/activation).

Structural promotion of ceria with alumina led to the formation of catalysts with higher specific surface areas and lower ceria crystallinity. While acid sites from γ-alumina were found to negatively affect the ammonia synthesis performance, basic alumina allowed to reduce the ceria loading while maintaining excellent activity and kinetic behaviour (activation energy as low as 44.8 kJ mol^{-1}) and reaction orders comparable to those of Ru/$CeO_2|_{AS}$.

The good performance of these easily prepared catalysts paves the way for a new family of 3rd generation catalysts which can be used as an alternative to complex electrides, hydrides and intermetallics, thereby providing new solutions for easier industrial catalyst scale up and effective integration of ammonia synthesis technology with renewables.

References

[1] M. Reese, C. Marquart, M. Malmali, K. Wagner, E. Buchanan, A. McCormick, E.L. Cussler, Ind Eng Chem Res 55 (2016) 3742–3750.

[2] H.H.T.V.S.G. Alfa Laval, Ammonfuel. An Industrial View of Ammonia as a Marine Fuel, 2020.

[3] K.H.R. Rouwenhorst, A.G.J. Van der Ham, L. Lefferts, Int J Hydrogen Energy 46 (2021) 21566–21579.

[4] C. Smith, A.K. Hill, L. Torrente-Murciano, Energy Environ Sci 13 (2020) 331–344.

[5] O.A. Ojelade, S.F. Zaman, Chemical Papers 75 (2021) 57–65.

[6] Q. Wang, J. Guo, P. Chen, Journal of Energy Chemistry 36 (2019) 25–36.

[7] F. Chang, W. Gao, J. Guo, P. Chen, Advanced Materials 33 (2021).
[8] M.L. Carreon, J Phys D Appl Phys 52 (2019) 483001.
[9] J. Hong, S. Prawer, A.B. Murphy, ACS Sustain Chem Eng 6 (2018) 15–31.
[10] S. Reichle, M. Felderhoff, F. Schüth, Angewandte Chemie - International Edition 60 (2021) 26385–26389.
[11] L. Li, T. Zhang, J. Cai, H. Cai, J. Ni, B. Lin, J. Lin, X. Wang, L. Zheng, C.T. Au, L. Jiang, J Catal 389 (2020) 218–228.
[12] J. Moon, Y. Cheng, L. Daemen, E. Novak, A.J. Ramirez-Cuesta, Z. Wu, Top Catal 64 (2021) 685–692.
[13] H. Yan, W. Gao, Q. Wang, Y. Guan, S. Feng, H. Wu, Q. Guo, H. Cao, J. Guo, P. Chen, Journal of Physical Chemistry C 125 (2021) 6716–6722.
[14] S. Wang, W. Yu, S. Xu, K. Han, F. Wang, ACS Sustain Chem Eng 10 (2022) 115–123.
[15] Y. Li, H. Wang, C. Priest, S. Li, P. Xu, G. Wu, Advanced Materials 33 (2021).
[16] J.M. McEnaney, A.R. Singh, J.A. Schwalbe, J. Kibsgaard, J.C. Lin, M. Cargnello, T.F. Jaramillo, J.K. Nørskov, Energy Environ Sci 10 (2017) 1621–1630.
[17] J. Humphreys, R. Lan, S. Tao, Advanced Energy and Sustainability Research 2 (2021) 2000043.
[18] V.S. Marakatti, E.M. Gaigneaux, ChemCatChem 12 (2020) 5838–5857.
[19] J. Arroyo-Caire, M.A. Diaz-Perez, M.A. Lara-Angulo, J.C. Serrano-Ruiz, Nanomaterials 2023, Vol. 13, Page 2914 13 (2023) 2914.
[20] C. Smith, L. Torrente-Murciano, Chem Catalysis 1 (2021) 1163–1172.
[21] H. Hosono, M. Kitano, Chem Rev 121 (2021) 3121–3185.
[22] N. Saadatjou, A. Jafari, S. Sahebdelfar, Chem Eng Commun 202 (2015) 420–448.
[23] L. Li, T. Zhang, Y. Zhou, X. Wang, C. tong Au, L. Jiang, Journal of Rare Earths 40 (2022) 1–10.
[24] Y. Nakaya, S. Furukawa, Chem Rev (2022).
[25] J. Guo, P. Chen, Acc Chem Res 54 (2021) 2434–2444.
[26] K. Sato, K. Nagaoka, Https://Doi.Org/10.1246/Cl.200855 50 (2021) 687–696.
[27] Y. Gong, H. Li, C. Li, X. Bao, H. Hosono, J. Wang, Journal of Advanced Ceramics 2022 11:10 11 (2022) 1499–1529.
[28] S. ichiro Miyahara, K. Sato, Y. Kawano, K. Imamura, Y. Ogura, K. Tsujimaru, K. Nagaoka, Catal Today 376 (2021) 36–40.
[29] Z. Ma, S. Zhao, X. Pei, X. Xiong, B. Hu, Catal Sci Technol 7 (2017) 191–199.
[30] M. Kitano, Y. Inoue, M. Sasase, K. Kishida, Y. Kobayashi, K. Nishiyama, T. Tada, S. Kawamura, T. Yokoyama, M. Hara, H. Hosono, Angewandte Chemie 130 (2018) 2678–2682.
[31] C. Fernández, C. Sassoye, D.P. Debecker, C. Sanchez, P. Ruiz, Appl Catal A Gen 474 (2014) 194–202.
[32] Z. Song, T. Cai, J.C. Hanson, J.A. Rodriguez, J. Hrbek, J Am Chem Soc 126 (2004) 8576–8584.
[33] P. Wang, F. Chang, W. Gao, J. Guo, G. Wu, T. He, P. Chen, Nat Chem 9 (2017) 64–70.

[34] H. Hosono, Catal Letters 152 (2022) 307–314.
[35] K. Ooya, J. Li, K. Fukui, S. Iimura, T. Nakao, K. Ogasawara, M. Sasase, H. Abe, Y. Niwa, M. Kitano, H. Hosono, Adv Energy Mater 11 (2021).
[36] M. Kitano, Y. Inoue, Y. Yamazaki, F. Hayashi, S. Kanbara, S. Matsuishi, T. Yokoyama, S.W. Kim, M. Hara, H. Hosono, Nat Chem 4 (2012) 934–940.
[37] Y. Gong, H. Li, J. Wu, X. Song, X. Yang, X. Bao, X. Han, M. Kitano, J. Wang, H. Hosono, J Am Chem Soc (2022).
[38] Y. Kobayashi, M. Kitano, S. Kawamura, T. Yokoyama, H. Hosono, Catal Sci Technol 7 (2017) 47–50.
[39] W. Li, P. Liu, R. Niu, J. Li, S. Wang, Solid State Sci 99 (2020) 105983.
[40] K. Sato, K. Imamura, Y. Kawano, S. ichiro Miyahara, T. Yamamoto, S. Matsumura, K. Nagaoka, Chem Sci 8 (2016) 674–679.
[41] X. Wang, X. Peng, Y. Zhang, J. Ni, C.T. Au, L. Jiang, Inorg Chem Front 6 (2019) 396–406.
[42] Z. Feng, F. Guo, Y. Zhang, T. Ichikawa, J. Zheng, Applied Catalysis B: Environment and Energy (2025) 125059.
[43] H.B. Kim, E.D. Park, Catal Today 411–412 (2023) 113817.
[44] M. Osozawa, A. Hori, K. Fukai, T. Honma, K. Oshima, S. Satokawa, Int J Hydrogen Energy 47 (2022) 2433–2441.
[45] J. Silvestre-Albero, F. Rodríguez-Reinoso, A. Sepúlveda-Escribano, J Catal 210 (2002) 127–136.
[46] B. Folkesson, M. Bjorøy, J. Pappas, S. Skaarup, R. Aaltonen, C.-G. Swahn, Acta Chem Scand 27 (1973) 287–302.
[47] M.M.T. Khan, S. Srivastava, Polyhedron 7 (1988) 1063–1065.

Graphical Abstract

Description

Differences in the apparent activation energy, specific surface area and support composition between catalysts made of Ru supported on commercial ceria, lab-synthesized ceria and basic ceria-alumina.